THE JOURNAL OF PHYSICAL CHEMISTRY C

ARTICLE

pubs.acs.org/JPCC

From Head to Tail: Structure, Solvation, and Hydrogen Bonding of Carboxylate Surfactants at the Organic−Water Interface

Daniel K. Beaman, Ellen J. Robertson, and Geraldine L. Richmond*

Department of Chemistry, University of Oregon, Eugene, Oregon, 97403 United States

ABSTRACT: From enhanced oil recovery to fertile soils and facial cosmetics, carboxylate containing organics are pervasive in our everyday lives. The carboxyl moiety whose charge and metal binding properties can be readily altered with pH often dictates the behavior of the organic to which it is attached. The focus of this study is on understanding how the carboxylate group controls the overall molecular behavior of two alkyl surfactants, Na-dodecanoate and Na-octanoate, at an oil−water interface. Detailed spectroscopic studies using vibrational sum frequency spectroscopy and interfacial tension measurements provide important new insights into the solvation, orientation, and hydrogen bonding of the adsorbed carboxylate headgroup and interfacial water in the oil−water boundary region and the influence of the attached alkyl tails on the surfactant characteristics. The results show that the molecular characteristics, from head to tail, are distinctly different than what has been observed for these surfactants at another hydrophobic/water interface, namely the air/water interface. This difference is attributed in large part to the solvating environment around the chains, which permits a more disordered monolayer and allows the carboxylates to adopt a wider variety of orientations at the interface and a larger number of hydrogen bonding scenarios.

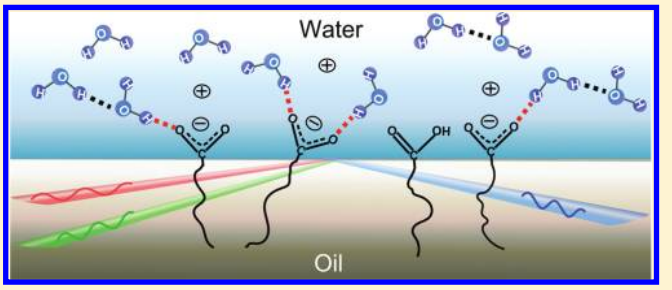

INTRODUCTION

Since ancient Babylonian times when soap-like materials were created for "washing the stones for servant girls",[1,2] carboxylate containing surfactants derived from the hydrolysis of fatty acids continue to be important today in industrial, commercial, and personal hygiene applications. In addition to being important in surfactant applications, carboxylate moieties are present in all amino acids, the basic building blocks of our most important biological macromolecules. Due to their overwhelming presence, their ability to be charged or neutral, and their hydrogen bonding character, they play an important role in many processes such as peptidyl transferase[3] and protein dynamics.[4] Carboxylates in the form of humic and formic substances bind to nutrients and toxins and thus have environmental implications with regards to transport through soils and water sheds.[5−7] Small carboxylic acid containing molecules are some of the most abundant organics found in fine particulate matter in the atmosphere. Thus their surface activity and ability to hydrogen bond at the surface of water droplets are of critical atmospheric importance.[8−10] Due to the abundant nature of the carboxylate functional group in these systems, understanding the aqueous solvating environment surrounding these functional groups at a wide variety of interfaces is of great importance due to the role the interface plays in these systems.

Carboxylic acid and carboxylate containing molecules at both the air−water[8,11−17] and the solid−liquid[18−21] interface have received much interest over the last two decades from surface specific techniques. IRRAS work by Gericke and co-workers focused on long chain carboxylic acids using a number of different metals to study binding effects and monolayer conformation.[15,22] Johann et al. used PMIRRAS to study similar monolayers as a function of pH.[23] While both of these studies were able to see splitting of the C═O vibrational mode into three distinct peaks due to hydrogen bonding, limited information was available about how the charged carboxylate headgroup was solvated at the air−water interface. Additionally, splitting of the asymmetric and symmetric carboxylate vibrational modes was seen by Johann et al., but there was no explanation as to why this occurred. Miranda and co-workers studied long chain carboxylic acids with vibrational sum frequency spectroscopy (VSFS) at the air−water interface and found that the surface pK_a is much different than what is normally found in bulk liquid.[12] Rao and co-workers also showed that surface pK_a is not equal to bulk pK_a in their VSFS work on phenolate ions at the air−water interface.[17] Allen and co-workers completed a study of carboxylic acids at the air−water interface in the presence of Na^+ and K^+ and found interesting frequency shifts due to binding of the ions with the carboxylates.[11] Tyrode et al. have completed a number of studies on carboxylates at the air−water interface, studying fluorinated carboxylate surfactants,[13] acetic acid,[24,25] and formic acid.[14] More recently in our laboratory, investigations of hexanoic acid at the air−water interface found interesting time dependent effects for the formed monolayer, which was

Received: March 3, 2011
Revised: May 12, 2011

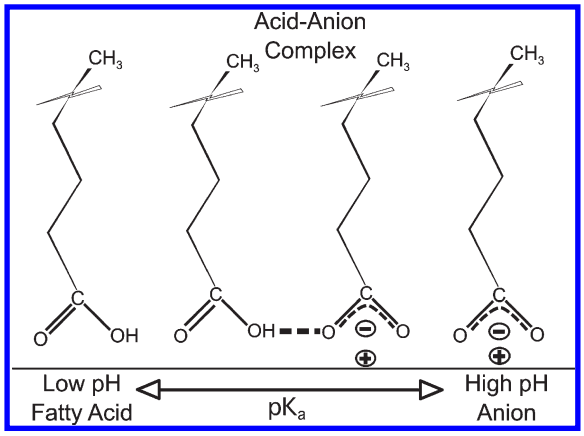

Figure 1. Carboxylate/carboxylic acid surfactants at low and high pH.

attributed to reorientation of the surface molecules.[8] This time dependence was observed to disappear upon the addition of salts. Carboxylate surfactants at the fluorite−water interface have also been investigated in studies of equilibrium and nonequilibrium dynamics of assemblies.[18,20] While many of these previous studies have used the headgroup vibrational modes to understand adsorption and metal binding, little attention has been paid to the solvating and hydrogen bonding environment of these charged carboxylate head groups at the surface. Nevertheless, from all of these past studies, it is clear that surfactant headgroup vibrational modes in the mid infrared region are rich in information and can be of valuable use in understanding the functionality of these important surfactants.

The oil−water interface provides a very different environment for surfactant adsorption relative to the air−water or solid−water interface. It is only recently that a molecular picture of this interface has begun to emerge, shedding light on the unique environment that this interface provides for surfactant and ion adsorption,[26−28] as well as nanoparticle assembly, polymer assembly, and interfacial reactions. What molecular level understanding of surfactant adsorption that exists has been almost exclusively focused on alkyl tail conformation upon adsorption.[28−30] This is the first study that explores the nature and bonding environment of the headgroup of a surfactant upon adsorption at the oil−water interface. Unlike what is observed at the air−water or solid−liquid interface where carboxylate headgroups have a highly defined orientation, we have found that these headgroups exist in a broad distribution of orientations at the oil−water interface. Direct evidence is provided for a multitude of coexisting hydrogen bonding coordinations that act to solvate the charged carboxylate headgroup at the CCl_4−water interface.

The surfactants examined in this paper are Na-dodecanoate (Na-Laurate) and Na-octanoate, with 12 and 8 carbons, respectively. Figure 1 shows the structure of these surfactants as surface films in their various states at different pHs. Literature reports give the pK_a of fatty acids in bulk water as ∼4−6.[11,12,19,31,32] Below the pK_a, the surface molecules exist as fatty acids and above the pK_a, they exists as a fully charged layer of anionic molecules. pH values near the pK_a produce an equilibrium between the charged and uncharged headgroup that can lead to acid−anion complexes.

EXPERIMENTAL SECTION

Spectroscopic Measurements. VSFS data was acquired with an Ekspla laser and IR generation system with a sample area built to accommodate the liquid−liquid cells and inverted beam geometries. This system has been described in detail elsewhere.[27] In short, a YAG laser outputs 1064 nm light with ∼30 ps pulse lengths. The 1064 nm light is split into two lines and one line is frequency doubled to give 532 nm light. A small portion of the 532 nm line is used as the visible portion at the interface, while the remainder of the 532 nm line and the 1064 nm line are used to generate tunable infrared light via a typical OPG/OPA/DFG setup. All data was taken with the visible and IR beams at 23.5° and 16°, respectively, from the plane of the interface.

The intensity of the detected sum frequency as shown in eq 1 is proportional to the square of the effective second order susceptibility, $\chi^{(2)}_{\text{eff}}$, and the intensity of the incident IR and visible beams.

$$I(\omega_{\text{sf}}) \propto |\chi^{(2)}_{\text{eff}}|^2 I(\omega_{\text{vis}}) I(\omega_{\text{IR}}) \quad (1)$$

The second order susceptibility, $\chi^{(2)}$, as shown in eq 2 and the effective second order susceptibility from eq 1 are related through the Fresnel coefficients and unit polarization vectors. Equation 2 shows that $\chi^{(2)}$ is composed of a nonresonant component and the sum of all present resonant components.

$$\chi^{(2)} = \chi^{(2)}_{\text{NR}} + \sum_{\nu} \chi^{(2)}_{\text{R}_\nu} \quad (2)$$

The resonant second order susceptibility, $\chi^{(2)}_{\text{R}_\nu}$ as shown in eq 3, is dependent on both the number density of the molecules at the interface as well as the molecular hyperpolarizability, β. The angled brackets around β indicate that this is an average over all possible molecular orientations in the probed system.

$$\chi^{(2)}_{\text{R}_\nu} = \frac{N}{\varepsilon_0} \langle \beta \rangle \quad (3)$$

The dependence of the sum frequency signal on both the number density at the interface and the molecular orientation provides a unique perspective on interfacial adsorption. In addition, the polarization of the generated sum frequency signal is dependent on the polarization of the visible and IR beams, and thus different polarization combinations can be used to probe different planes of the interface. In this study, polarization combinations ssp, sps, and ppp are used and the order of each polarization combination goes as the sum frequency, visible, and IR, respectively. The polarization combination of ssp is used to probe components of the dipole that lie normal to the interfacial plane, whereas sps is used to probe components of the dipole that are in the plane of the interface, and ppp is sensitive to components that are both in and out of the plane of the interface.

The sample cell was designed from a solid piece of Kel-f and contains two windows set normal to the incident and outgoing 532 nm beam and are sealed with Dupont Kalrez perfluoropolymer O-rings. The input windows was CaF_2 and the output window was BK-7 glass as it only needed to transmit the generated visible wavelength sum-frequency light, and it was more robust toward the aggressive cleaning process used. All glassware, the cell, the BK-7 window, and the O-rings were soaked in concentrated sulfuric acid with No-Chromix for a minimum of 12 h and then each piece was rinsed under water from an 18 MΩ Nanopure filtration system for at at least 25 min. The CaF_2 window was allowed to soak in the same acidic solution for 15−20 min and then copiously rinsed.

Data acquisition started immediately after the interface was made and usually continued for approximately an hour for each prepared interface. Each spectra shown in these experiments is an

dx.doi.org/10.1021/jp202061y |J. Phys. Chem. C XXXX, XXX, 000–000

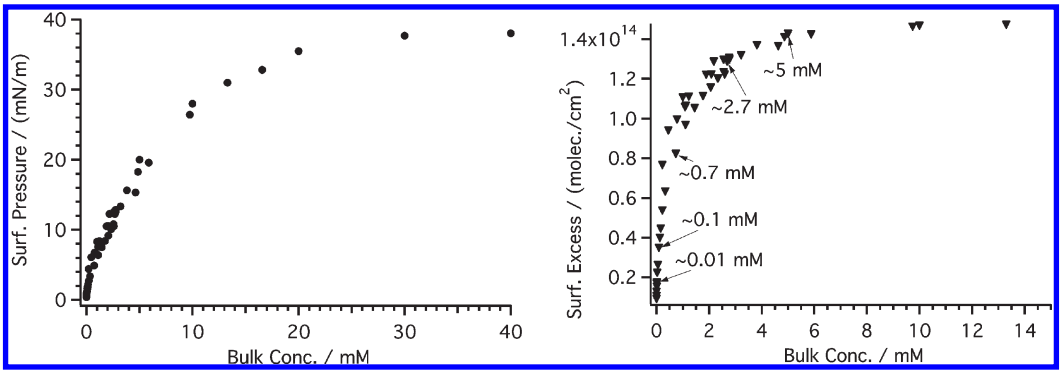

Figure 2. Interfacial tension data acquired with the Wilhelmy plate and pendant drop method (left) and the corresponding calculated surface excess (right) of Na-dodecanoate at the CCl_4—water interface. The data points marked in the surface excess plot are approximately the concentrations used in the spectroscopy experiments.

average of at least 300 laser shots per data point. In the cases where equilibration of the VSFS signal was not immediately achieved, only the spectra taken at post equilibrium were averaged. Long-term equilibration was checked by letting the interface sit for 6 to 12 h and then retaking the spectra. In all cases there was no long-term time dependence observed in the spectroscopic data.

Sample Preparation. Chemicals were purchased in the highest purity possible from Sigma-Aldrich (Na-dodecanoate 99—100%, Na-octanoate 99%, and NaOH 1.0 N solution in water) and CDN Isotopes (d-K-dodecanoate 98.7% atom d). To avoid any doubt about the contributions to the spectra based on the purity of the deuterated sample, it was tested via TOF-SIMS and was found to be of high enough purity that contributions to surface structure from C—H groups would be less than 1/100 of their C-D counterparts, thus allowing easy distinction between mid-IR CH vibrational modes and other vibrational modes on the molecule when the deuterated compounds were substituted. Solutions were prepared using clean glassware, an analytical balance and water from a Barnstead Nanopure system. To study solutions containing all carboxylate anion, the solutions were always adjusted to pH 10 (far above the pK_a) using NaOH and tested using EMD pH paper with regular verification via an Oakton 110 series pH meter.

Interfacial Tension. Interfacial tension experiments were carried out to support the VSFS experiments. To obtain the highest degree of accuracy, measurements were taken on two different types of tensiometers: a balance type that uses the Wilhelmy plate method (KSV) and an optical tensiometer that uses the pendant drop method (KSV). For the Whilhelmy plate method, a CCl_4-water interface is prepared and verified to be clean with the balance. To obtain interfacial tension data for different surfactant concentrations, aliquots of a stock solution of surfactant that was also pH adjusted to 10, were added to the aqueous phase (also pH adjusted) and allowed to equilibrate. Interfacial tension data was recorded when the surface tension did not drift more than 0.2 mN/m for 5 min. For the pendant drop method, a drop of water in CCl_4 was prepared and the neat interfacial tension value verified. A pendant drop was then made using the specified solution. Data was recorded at 1 min intervals until no change was seen in the drop. Interfacial tension values were then calculated via the KSV software using the acquired images. Both instruments were found to give overlapping data and the plots shown in these experiments contain data from both instruments.

RESULTS AND DISCUSSION

Interfacial Tension Measurements. Knowing the surface concentration is important to the VSFS experiments because a change in the spectroscopic signal can occur for a variety of reasons in addition to surface concentration changes, including loss of orientation or signal cancellation from the formation of a bilayer at the interface. Combining the spectroscopy data with the interfacial tension results allows a more complete picture of the formation of a monolayer to be built. Our interfacial tension measurements with the Wilhelmy plate method and the pendant drop method were found to agree within error. The interfacial tension of Na-dodecanoate at the CCl_4—water interface is shown in Figure 2 and is typical in shape compared with other surfactants adsorbed at the oil—water interface. The data shown gives a CMC value of ~27 mM which is consistent with past literature CMC values for Na-dodecanoate.[33,34] The limiting surface coverage, Γ_i, can be calculated using the Gibbs equation:[34]

$$\Gamma_i = \frac{1}{n_i RT}\left(\frac{\partial \Pi}{\partial \ln a_i}\right)_T \quad (4)$$

where n_i is the number of solute species at the interface that change when bulk concentration is changed, Π is the interfacial pressure, and a_i is the activity. For sufficiently dilute solutions of surfactant such as those used in these investigations, the activity can be replaced by the bulk concentration. Γ_i for Na-dodecanoate at the CCl_4—water interface was calculated to be 67 Å^2/molecule. When compared with literature values of solutions of carboxylate surfactants at the air—water and oil—water interface near the pK_a, this value is larger than what has been reported by 15—20 Å^2.[34] The main reason for the larger value in these experiments is the higher pH of 10, which gives surfactant solutions with the headgroup predominantly in its anionic form. As a result, charge—charge repulsion between head groups increases the area per molecule. From the interfacial tension data and the limiting surface excess value, the surface excess, at any bulk concentration can be calculated using the Frumkin equation:[34]

$$\Pi = -RT\Gamma_i \ln\left(1 - \frac{\Gamma_2}{\Gamma_i}\right) \quad (5)$$

where Γ_2 is the surface excess at a given interfacial pressure corresponding to a bulk concentration. Figure 2 shows the surface excess (right) for Na-dodecanoate at the CCl_4—water interface.

dx.doi.org/10.1021/jp202061y |J. Phys. Chem. C XXXX, XXX, 000–000

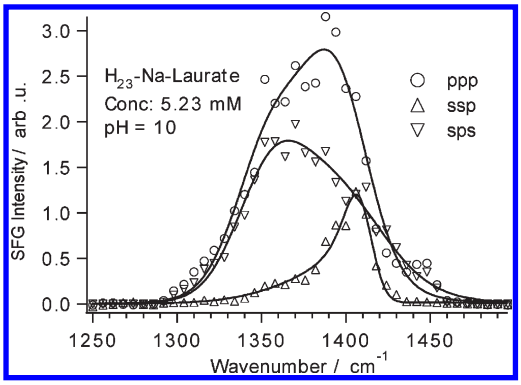

Figure 3. Polarization schemes ppp (○), ssp (△), and sps (▽) of Na-dodecanoate with a fully protonated chain at a concentration of 5.23 mM which is equivalent to a full monolayer at the interface according to interfacial tension data. Solid lines are fits to the data. Spectral intensity is not quantitatively comparable across-polarizations.

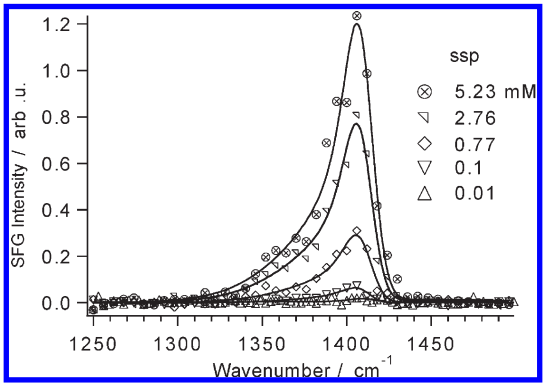

Figure 4. Concentration series of Na-dodecanoate in the ssp polarization scheme at pH 10. Equivalent concentrations in this figure and Figure 5 have the same data symbols. 0.01 mM (△) was not able to be fit accurately due to the very low signal count obtained. Solid lines are two-peak fits to the data.

Five bulk concentrations (shown in Figure 2) have been chosen to allow investigation from the dilute surface concentration regime, up to the full monolayer regime. From this figure, it is seen that a full monolayer is achieved at ∼4.5 mM bulk concentration. Beyond this bulk concentration, no additional adsorption of the surfactant at the interface is observed.

VSFS of Na-Dodecanoate at CCl_4−Water Interface. VSFS experiments were used to probe the adsorption and ordering of Na-dodecanoate at different levels of surface coverage as obtained by the interfacial tensions measurements. Figure 3 shows the VSF spectra of a full monolayer of Na-dodecanoate at the CCl_4−water interface in ssp, sps, and ppp polarization schemes. Several general conclusions can be drawn from these spectra prior to the more detailed spectral analysis and fitting that follows later in the paper. Strong intensity with considerate breadth is found around 1400 cm^{-1} in the region of the symmetric vibrational mode of COO^-. Signal was not observed for the asymmetric stretch under any polarization combination. The three polarization spectra provide insight into the number of modes present in the spectra and their different relative geometries. The ssp spectrum shows a peak centered at 1410 cm^{-1} with a tailing shoulder on the low energy side. In contrast, the sps

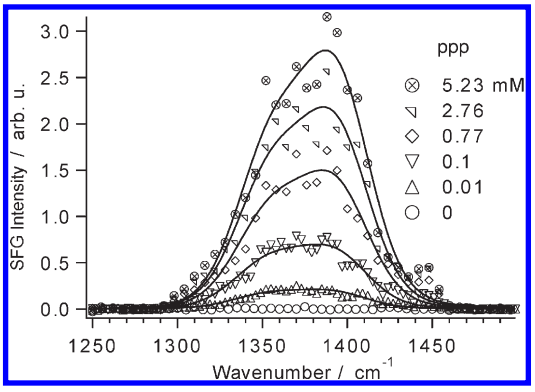

Figure 5. Spectral series showing a concentration range of Na-dodecanoate in the ppp polarization scheme at pH 10. Zero mM concentration (○) is added for reference to demonstrate a scan of the CCl_4−water interface in this region with no surfactant added. Solid lines are two-peak fits to the data.

spectrum shows a peak at 1365 cm^{-1} with a large shoulder on the high energy side. The combination of these two polarization schemes clearly lead us to conclude that there are two dominant peaks present in the VSF spectra. The higher energy peak in the ssp polarization spectra shows a higher amplitude than the lower energy peak, opposite of what is found for sps. This indicates different overall orientational geometry for these two modes since ssp and sps probe dipole components that are orthogonal to each other. These intensity trends lead us to conclude that the lower frequency peak at 1365 cm^{-1} has a significant dipole contribution in the plane of the interface due to its larger amplitude in sps than in ssp. The higher frequency peak at 1410 cm^{-1} has a significant component normal to the interface as it is dominant in ssp. The ppp polarization is a combination of four elements of $\chi^{(2)}_{ijk}$ and shows both of the vibrational modes with a different trend than what is observed in ssp or sps. The ssp (sps) spectra show a small amount of the low frequency (high frequency) peak because those contributing dipole moments are not exclusively parallel (perpendicular) to the interface, thus they will have a small component projected into the perpendicular (parallel) plane which will be picked up by the ssp (sps) polarization scheme.

A concentration series for ssp polarization combination is shown in Figure 4. A clear dominant mode is observed to grow in at ∼1405 cm^{-1} with a small shoulder on the low energy side at ∼1365 cm^{-1}. Figure 5 shows the analogous spectra in the ppp polarization scheme. In this case, the lower frequency component of the spectra is clearly observed. The two peaks together are very broad for all concentrations studied, spanning ∼75 cm^{-1} fwhm. VSF spectra in ppp polarization gives more signal than ssp and the lower concentrations are more clearly resolved, which will have consequences for the spectral analysis discussed in the next section. In addition to the COO^- mode, IR, and Raman spectra of carboxylate surfactants in the spectral region of Figure 3 also contain several CH bending, wagging, and deformation modes.[35] Distinguishing the modes can be facilitated by deuteration of the surfactant chain to isolate the headgroup vibration in the 1400 cm^{-1} region. Figure 6 shows the VSFS results of a fully deuterated chain of K-dodecanoate. The similarity of the spectrum in Figure 6 with Figure 3 confirms that the full spectral region studied here is due solely to the carboxylate headgroup modes. The change in counterion from

dx.doi.org/10.1021/jp202061y |J. Phys. Chem. C XXXX, XXX, 000–000

Na^+ to K^+ is the cause for the difference in amplitudes between the protonated and deuterated hydrocarbon chains as verified by the addition of excess K^+ to the Na-dodecanoate (spectra not shown) which causes the amplitudes to increase as seen for the D_{23}-K-dodecanoate spectra.

Spectral Analysis and Mode Assignment. To understand the contributing surfactant species to the overall spectra and to determine the spectral characteristics of the two dominant peaks, spectral fitting routines have been applied. As shown in eq 2 VSFS spectral intensity is related to the square of $\chi^{(2)}_{NR}$ and $\chi^{(2)}_{R_\nu}$, and thus interferences can occur between the nonresonant background and the resonant modes, as well as between adjacent resonant modes. Due to these interferences, the spectra must be fit in order to gain accurate information such as amplitudes, center position, and phase. To fit the spectra, a convolution of a Lorentzian and a Gaussian taking the form of eq 6 allows both homogeneous and inhomogenous broadening to be taken into account.[36]

$$|\chi^{(2)}(\omega_{SF})|^2 = \left|\chi^{(2)}_{NR} + \int_{-\infty}^{\infty} \frac{A_\nu}{\omega_L - \omega_{IR} - i\Gamma_L} \exp\left[-\frac{(\omega_L - \omega_\nu)^2}{\Gamma_\nu^2}\right] d\omega_L\right|^2 \quad (6)$$

In order to take a rigorous approach to fitting, a global routine was used for the ssp and ppp concentration series shown in Figures 4 and 5. In these cases all parameters are global except the amplitudes, which allows a higher confidence in the results versus fitting each individual spectrum separately. The result is that all spectra can be fit accurately with two peaks that will be referred to as ν_1 and ν_2 for the lower and higher frequency peaks, respectively.

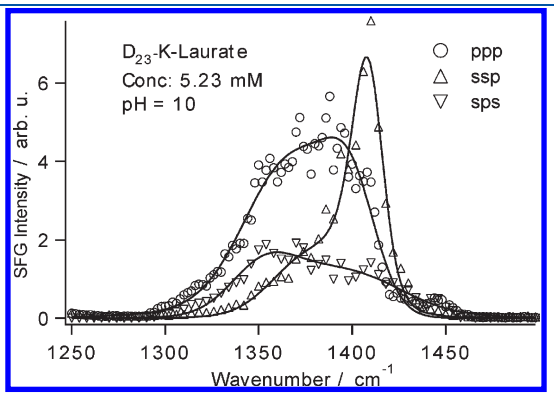

Figure 6. Polarization schemes ppp (○), ssp (△), and sps (▽) of K-dodecanoate with a fully deuterated chain at a concentration of 5.23 mM. Solid lines are two-peak fits to the data.

From the global fits, the amplitudes from the concentration series are useful in determining the adsorption properties of the monolayer. The two contributions to spectral intensity are number density of the molecules at the interface, and the average orientation of those molecules (eq 3). By combining the resulting surface concentrations from the interfacial tension data and the amplitudes from the spectral global fits, it is possible to probe conformational changes during the formation of the monolayer. In Figure 7, the square root of the intensity is plotted with respect to the surface concentration for both the low and high frequency peaks in the ssp spectral series. When plotted and fit to a line, the amplitudes clearly show a monotonic increase with respect to surface concentration indicating that the increase in VSFS signal is due to the effect of increasing number density at the interface and not a change in orientation as the monolayer is forming. The lowest concentration in ssp could not be reliably fit due to the low signal strength. When the ppp amplitudes are plotted in a similar fashion, roughly the same trend is observed with the lowest concentration being the exception. In Figure 7, it is seen that above ~0.4×10^{14} molecules/cm^2 (250 Å^2/molecule) the trend is quite linear for both the low and high frequency modes in ssp and ppp. The nonlinearity for the lowest concentration ppp amplitude indicates that at very low surface coverage, there is a change in orientation as the surface number density increases but only up to the concentration of ~0.4×10^{14} molecules/cm^2. Beyond this surface concentration, the monolayer continues to form monotonically without any significant changes in overall orientation. This is not unexpected given that, at very low surface coverage, monolayers are known to have large areas per molecule and thus less conformational order comes from decreased chain−chain interactions which would result in an initial "floppy" headgroup.[28,30] One interesting observation from comparison of the concentration data in Figure 7 for the two polarizations is the consistently higher slope for the higher frequency peak. This peak is the one corresponding to the more upright carboxylate configuration. Assuming similar transition probabilities for modes contributing to these peaks, the results indicate that the upright configuration is favored over the low frequency mode with more character in the plane of the interface.

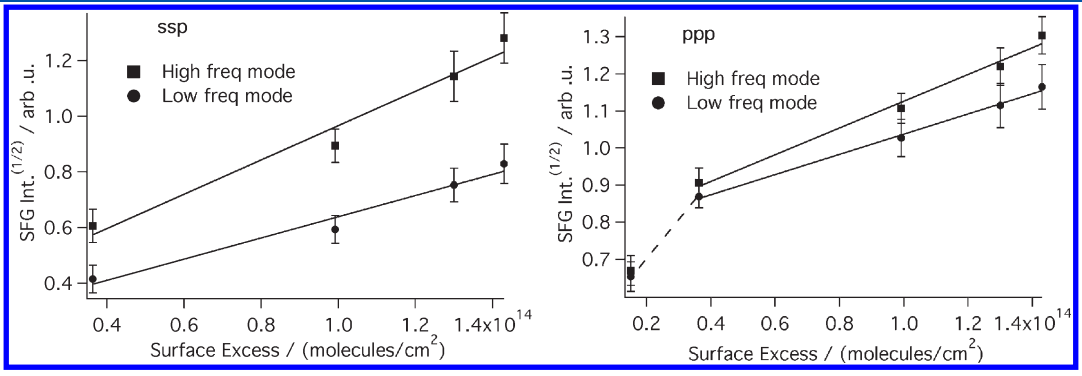

Figure 7. Square root of the fit intensity in the ssp (left) and ppp (right) polarization scheme from Figures 4 and 5, plotted against the surface concentration from Figure 2. Each data point represents the center frequency for the low (●) or high (■) frequency mode at that particular surface concentration. The solid line is a linear fit to the data and the error bars are the standard deviation from fitting the preaveraged individual sets of concentration spectra. The dotted line is to illustrate the change in linearity below a surface coverage of 0.4×10^{14} molecules/cm^2.

dx.doi.org/10.1021/jp202061y |J. Phys. Chem. C XXXX, XXX, 000–000

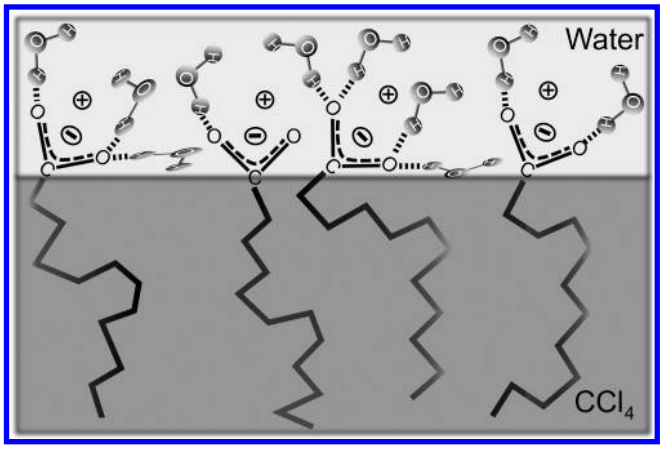

Figure 8. Representative cartoon showing the variety of structures and orientations of the headgroups at the oil−water interface.

One of the most interesting characteristics of the spectra corresponding to the COO^- ν_s modes of the adsorbed carboxylate surfactant is the spectral breadth, which indicates that there is a broad distribution of frequencies for the headgroup. This distribution fits into two distinct frequency regions, one centered at ∼1365 cm^{-1} and one at ∼1405 cm^{-1}, both of which have widths between 25 and 30 cm^{-1}. At the air−water interface for carboxylate surfactants,[11,13] a single narrow peak for the COO^- symmetric stretch is observed at 1410 cm^{-1}. We attribute these differences to the unique attributes of the oil−water interface. The main difference between the oil−water and air−water interface is that the hydrocarbon chains of the surfactants are fully solvated by the oil phase and thus the chain−chain interactions are minimized resulting in a more disordered monolayer than at the air−water interface.[28] In conjunction with the solvated chains, the large area per headgroup due to the charge−charge repulsion between neighboring surfactants further contributes to disorder in the adsorbed surfactant layer. This large area per headgroup combined with the solvation of the chains allows the molecules at the interface to adopt a wide variety of orientations and conformations, which allows the headgroup to have a broad distribution of angles at the interface. This distribution falls into two distinct angular regions. Based on the distribution of frequencies in the spectra, we predict that the headgroup exists in a variety of hydrogen bonding structures at the interface, each with a unique coordination number to the nearby water molecules. Each carboxylate headgroup has four total possible hydrogen bonding opportunities with nearby water, two to each oxygen. However, not every headgroup will be bound the maximum number of times. Headgroups that are less bonded to water will have a higher vibrational frequency due to less damping of the COO^- ν_s. We assign these less bound headgroups to the mode at 1405 cm^{-1} . More water bound headgroups will have a lower vibrational frequency, and we assign these to the 1365 cm^{-1} mode. The orientation and water bonding configuration is illustrated in Figure 8 for the headgroup at the CCl_4−water interface.

As observed in Figures 3 and 6, the lower frequency peak is more prominent in the sps spectra, indicating that the dipole of the headgroup is more in the plane of the interface than normal to it. MD simulations suggest that a large percentage of interfacial water molecules are not actually sum frequency active because they lie in the plane of the interface and are largely isotropic.[37,38]

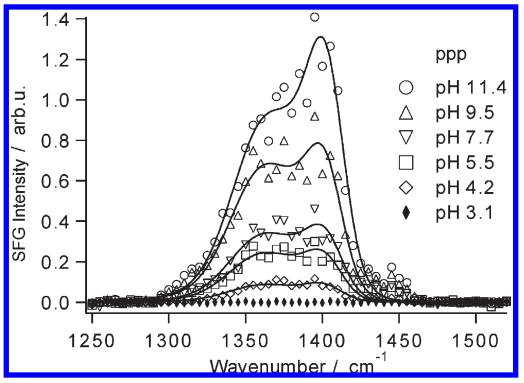

Figure 9. VSF spectra of the Na-octanoate headgroup at 5 mM in ppp polarization from pH 11.4 down to pH 3.1.

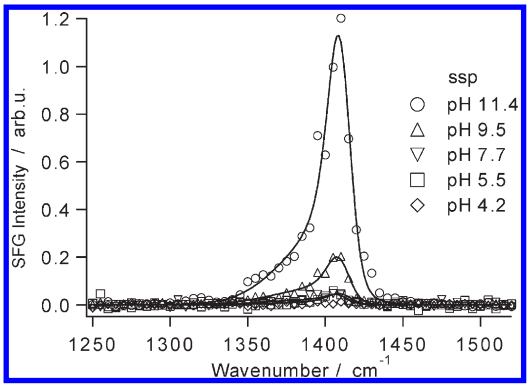

Figure 10. VSF spectra of the Na-octanoate headgroup at 5 mM in ssp polarization from pH 11.4 down to pH 4.2.

This makes it more likely that a carboxylate headgroup with one of it is oxygens near the plane of the interface would have more bonding opportunities with these "in plane" water molecules, which leads to the picture in Figure 8. While only two vibrational modes can be resolved spectroscopically, Figure 8 shows the extent of possible configurations that would exist at the interface. The higher frequency peak at 1405 cm^{-1} is assigned to carboxylate headgroups that have their dipole more normal to the interface and are hydrogen bound less than their lower frequency counterparts.

Effect of pH on Surfactants at the Interface. Carboxylic acids are weak acids and are therefore sensitive to the pH of the surrounding environment. The pH at an interface is often significantly different than in the bulk due to the increased concentration of hydronium ion.[39−41] This leads to surfactant interfacial pK_a values that vary widely from their bulk counter parts. Figures 9 and 10 show VSF spectra of Na-octanoate in ppp and ssp polarization as a function of pH. It is evident that as pH decreases, the entire contribution to the signal in both ssp and ppp decreases as well, indicating that all interfacial carboxylates with their associated orientations adopt a proton to the same degree. Figure 11 presents the water and CH vibrational region of the spectrum for Na-octanoate adsorbed at the CCl_4−water interface. The two primary regions of interest are the CH stretching region from 2800−3000 and 3000−3800 cm^{-1}, which is associated with the water vibrational modes. Combining the headgroup information gained from the mid-IR region with VSF spectra from the water region, it is observed that even at low pH

dx.doi.org/10.1021/jp202061y |J. Phys. Chem. C XXXX, XXX, 000–000

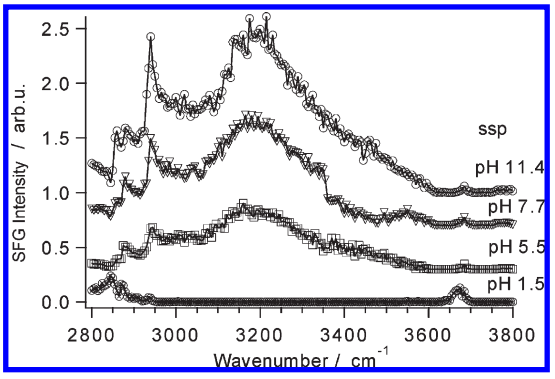

Figure 11. VSF spectra of the water and CH region for Na-octanoate adsorbed at the CCl_4−water interface in ssp polarization. Spectra are offset for clarity.

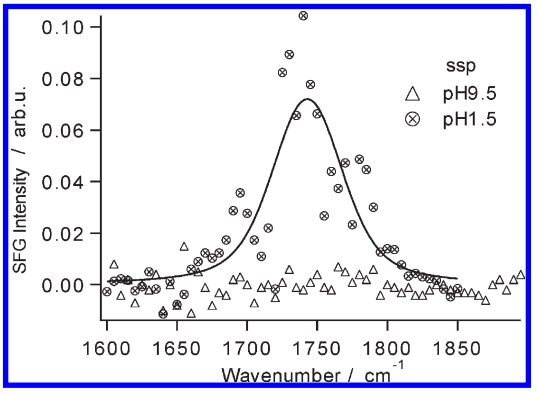

Figure 12. VSF spectra of the carbonyl band from octanoic acid at 1740 cm^{-1}.

there is a small amount of CH signal, showing that surfactant is still present at the interface, although in very low quantities. This is supported by interfacial tension results of Na-octanoate at 5 mM, which give values of ∼37, 43, and 44 mN/m for pH 10, 5, and 1.5 respectively. Given the neat CCl_4−water interfacial tension value of ∼44.5 mN/m, it clearly demonstrates there is very little adsorption of the carboxylic acid form of the surfactant at low pH. Figure 12 presents the C═O vibrational stretch in the 1700 cm^{-1} region for low and high pH. At low pH (<3), the surfactant is fully protonated as evidenced by the lack of signal in the 1400 cm^{-1} region in Figures 9 and 10, and the presence of C═O signal at ∼1740 cm^{-1} in Figure 12. In addition, the lack of water signal at low pH in Figure 11 provides further support for a fully protonated surfactant at the interface because a fully protonated monolayer of surfactants would provide a neutral field at the CCl_4−water interface and thus there would be few oriented water molecules.[42] At high pH, when the headgroup is deprotonated and charged, a field is created at the interface due to the double layer effect which acts to align the water molecules with the field at the surface. This is manifested in the spectra by the large peak at 3200 cm^{-1}, which is typical of more highly coordinated water molecules at the interface.[43] The data at low pH suggests the opposite picture where a majority of the headgroups are protonated, and the lack of a field at the interface from charge neutrality leads to the loss of water signal at 3200 cm^{-1}. Evidence for the presence of surfactant at the interface at both high and low pH is given by the C−H modes in the 2800−3000 cm^{-1} region as well as the headgroup modes in both the 1400 and 1700 cm^{-1} region. Interestingly, there is a stronger propensity for the charged headgroup to be at the interface as evidenced by its stronger signal relative to the weak C═O mode seen in Figure 12 corresponding to the protonated headgroup. The explanation for the low C═O signal of the carboxylic acid groups at the interface is 2-fold. First, there is a small number of carboxylic acid headgroups at the interface as shown by the interfacial tension measurements. This is additionally supported by the appearance of the free OH near 3700 cm^{-1}, which would only appear if the surfactant population were low.[44] In addition, the low CH signal in Figure 11 that indicates some surfactant is present negates the argument that there is simply in plane cancellation of the C═O mode. Given that the area per headgroup at the interface must be significantly larger with the lower numbers of carboxylic acids, the second contribution to low signal is that the few carboxylic acid headgroups at the interface are not well oriented and thus give a much smaller signal per headgroup. In addition, the IR transition moment would clearly be different if a carboxyl group and a carboxylic acid were both oriented normal to the interface. The carbonyl stretch would have its transition moment not normal to the interface whereas the carboxylate symmetric stretch would have its transition moment perfectly normal to the interface. This combination of factors leads to low SF signal for the carbonyl mode.

Comparison with Carboxylates at Other Interfaces. Comparing the vibrational frequencies of the carboxylate headgroup at the oil−water interface with carboxylate frequencies at the CaF_2−water and air−water interface provides insight to the water molecules solvating the headgroup and the location of the headgroup within the oil−water interface. Figure 13 tabulates the frequencies observed for carboxylate headgroups with varying chain length at the CaF_2−water interface,[20] and shows how the frequencies observed at the air−water and oil−water interface compare. At the CaF_2−water interface, an increase in chain length corresponds to increased hydrophobic interactions, resulting in fewer water molecules penetrating the surfactant tails and solvating the headgroup. Decreasing water solvation around the headgroup leads to less vibrational damping of the COO^- symmetric stretch, resulting in higher vibrational frequencies. At the air−water interface, the vibrational frequency of the carboxylate symmetric stretch is typically observed between 1405 and 1415 cm^{-1} for long chain surfactants.[13,35,45−47] Strong chain−chain interactions between the surfactant tails pointing into the vapor phase leads to a well oriented monolayer with highly structured tails and headgroups.[48,49] The resulting vibrational frequency for the carboxylate symmetric stretch at the air−water interface is lower than all but the smallest molecule (formate) at the CaF_2−water interface. This indicates that at the air−water interface, a higher degree of water solvation exists around the headgroup than most of the carboxylates shown for the CaF_2−water interface in Figure 13. At the CCl_4−water interface, the lower of the two vibrational peaks corresponding to the COO^- symmetric stretch (ν_1), is observed with a center frequency very near that of formate at the CaF_2−water interface. We conclude that these carboxylate headgroups are highly solvated by water molecules at the CCl_4−water interface, even more so than the highly oriented carboxylate headgroups at the air−water interface. The higher frequency carboxylate vibration at the CCl_4−water interface (ν_2), is more comparable to the carboxylates at the air−water interface, both in its orientation and water solvation. We conclude the low vibrational frequencies at the CCl_4−water interface are due to the chains being solvated by the

dx.doi.org/10.1021/jp202061y |J. Phys. Chem. C XXXX, XXX, 000–000

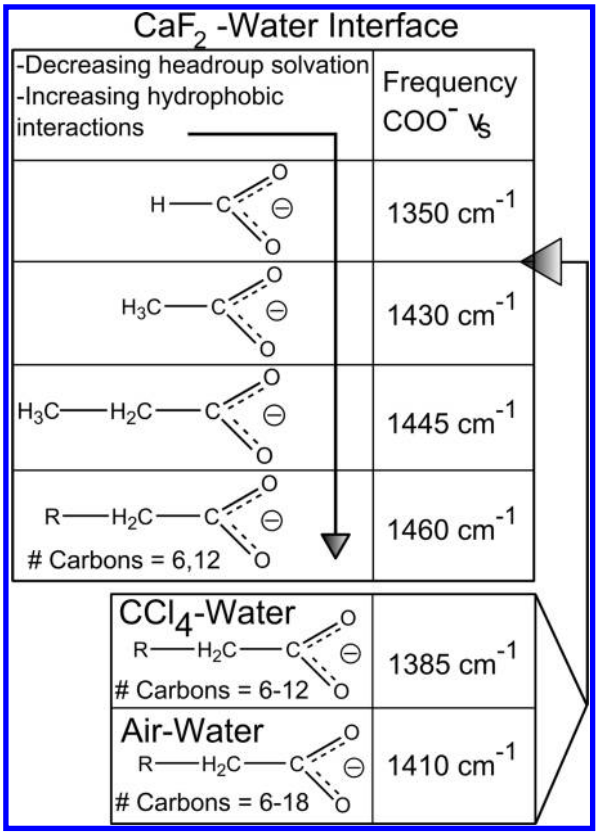

Figure 13. COO^- ν_s frequencies of carboxylate surfactants with increasing chain lengths at the CaF_2—water interface (top table) and the COO^- ν_s frequencies of Na-dodecanoate at the air—water and CCl_4—water interface (lower table). Clearly the trend is increased vibrational frequency with increased hydrophobic interactions. The air—water and oil—water vibrational frequencies of a 12 carbon chain fall near the "very little hydrophobic interactions" side of of the CaF_2 table. CaF_2 frequencies obtained from ref 20.

oil phase, which allows the headgroups to adopt an orientation where solvation by surface water molecules is maximized and the symmetric stretch is damped. Furthermore, we conclude that the headgroups corresponding to ν_2 with less solvating water molecules are located closer to the organic phase than those corresponding to ν_1, due to less water molecules being available for hydrogen bonding to the headgroup the further into the oil phase they are located.

CONCLUSIONS

Carboxylates are one of the most prevalent functional groups, existing throughout a wide variety of chemical and biological systems. While carboxylates and carboxylic acids have received a wide array of both experimental and theoretical attention in bulk liquids, there is still much to be understood about these functional groups at interfaces. This is the first study to investigate the bonding environment of a carboxylate surfactant headgroup at the oil—water interface. By monitoring the corresponding properties of the alkyl chains and interfacial water, an integrated picture of the surfactant at the oil—water interface is achieved. We find that the surfactant takes on more freedom of motion at this interface, resulting in the headgroup adopting a range of orientations and degrees of solvation. We attribute this to the alkyl chains being solvated in the oil phase, creating a more fluid monolayer. This allows the headgroup to maximize its interactions with water at the interface, and results in a wide variety of hydrogen bonding configurations between the headgroup and water molecules. We find that the carboxylate headgroup at the oil—water interface is more highly solvated by water molecules than at either the air—water or solid—liquid interface. pH dependence shows the acid form of the headgroup to be less prevalent at the interface and not well oriented, illuminating the strong propensity of a charged headgroup to be drawn to the oil—water interface. Given the broad distribution of headgroup orientations and resulting hydrogen bonding structure, studies of carboxylates at the oil—water interface would help enlighten the complexity behind the nature of counterion binding at interfaces. Studies revolving around this topic are currently underway in our laboratory.

AUTHOR INFORMATION

Corresponding Author

*E-mail: richmond@uoregon.edu. Fax: 541-346-3422. Phone: 541-346-0116.

ACKNOWLEDGMENT

This material is based upon work supported by the National Science Foundation under CHE-0652531.

REFERENCES

(1) Butler, H.; Poucher, W. A. *Poucher's perfumes, cosmetics and soaps*, 10th ed.; Kluwer Academic Publishers: Boston, 2000.
(2) Levey, M. *Isis* **1958**, *49*, 341.
(3) Naughton, M. A.; Dintzis, H. M. *Proc. Natl. Acad. Sci.* **1962**, *48*, 1822–1830.
(4) Checover, S.; Marantz, Y.; Nachliel, E.; Gutman, M.; Pfeiffer, M.; Tittor, J.; Oesterhelt, D.; Dencher, N. A. *Biochemistry* **2001**, *40*, 4281–4292.
(5) Rebhun, M.; Meir, S.; Laor, Y. *Environ. Sci. Technol.* **1998**, *32*, 981–986.
(6) Stathi, P.; Louloudi, M.; Deligiannakis, Y. *Environ. Sci. Technol.* **2007**, *41*, 2782–2788.
(7) Buschmann, J.; Kappeler, A.; Lindauer, U.; Kistler, D.; Berg, M.; Sigg, L. *Environ. Sci. Technol.* **2006**, *40*, 6015–6020.
(8) Kido, M. C.; Blower, P. G.; Richmond, G. L. *J. Phys. Chem. B* **2007**, *111*, 13703–13713.
(9) Russell, L. M.; Maria, S. F.; Myneni, S. C. B. *Geophys. Res. Lett.* **2002**, *29*, 1–4.
(10) Saxena, P.; Hildemann, L. M. *J. Atmos. Chem.* **1996**, *24*, 57.
(11) Tang, C. Y.; Allen, H. C. *J. Phys. Chem. A* **2009**, *113*, 7383–7393.
(12) Miranda, P. B.; Du, Q.; Shen, Y. R. *Chem. Phys. Lett.* **1998**, *286*, 1–8.
(13) Tyrode, E.; Johnson, C. M.; Rutland, M. W.; Day, J. P.; Bain, C. D. *J. Phys. Chem. C* **2007**, *111*, 316–329.
(14) Johnson, C. M.; Tyrode, E.; Kumpulainen, A.; Leygraf, C. *J. Phys. Chem. C* **2009**, *113*, 13209–13218.
(15) Gericke, A.; Huhnerfuss, H. *J. Phys. Chem.* **1993**, *97*, 12899–12908.
(16) Gurau, M. C.; Kim, G.; Lim, S.; Albertorio, F.; Fleisher, H. C.; Cremer, P. S. *Chem. Phys. Chem.* **2003**, *4*, 1231–1233.
(17) Rao, Y.; Subir, M.; McArthur, E. A.; Turro, N. J.; Eisenthal, K. B. *Chem. Phys. Lett.* **2009**, *477*, 241–244.
(18) Becraft, K. A.; Richmond, G. L. *J. Phys. Chem. B* **2005**, *109*, 5108–5117.
(19) Konek, C. T.; Musorrafiti, M. J.; Al-Abadleh, H. A.; Bertin, P. A.; Nguyen, S. T.; Geiger, F. M. *J. Am. Chem. Soc.* **2004**, *126*, 11754–11755.

(20) Schrodle, S.; Moore, F. G.; Richmond, G. L. *J. Phys. Chem. C* **2007**, *111*, 8050–8059.
(21) Winter, N.; Vieceli, J.; Benjamin, I. *J. Phys. Chem. B* **2007**, *112*, 227–231.
(22) Kutscher, J.; Gericke, A.; Huhnerfuss, H. *Langmuir* **1996**, *12*, 1027–1034.
(23) Johann, R.; Vollhardt, D.; Mohwald, H. *Colloids Surf. A* **2001**, *182*, 311–320.
(24) Johnson, C. M.; Tyrode, E.; Baldelli, S.; Rutland, M. W.; Leygraf, C. *J. Phys. Chem. B* **2005**, *109*, 321–328.
(25) Tyrode, E.; Johnson, C. M.; Baldelli, S.; Leygrad, C.; Rutland, M. W. *J. Phys. Chem. B* **2005**, *109*, 329–341.
(26) McFearin, C. L.; Beaman, D. K.; Moore, F. G.; Richmond, G. L. *J. Phys. Chem. C* **2009**, *113*, 1171–1188.
(27) McFearin, C. L.; Richmond, G. L. *J. Phys. Chem. C* **2009**, *113*, 21162–21168.
(28) Watry, M. R.; Richmond, G. L. *J. Am. Chem. Soc.* **2000**, *122*, 875–883.
(29) Conboy, J. C.; Messmer, M. C.; Richmond, G. L. *J. Phys. Chem.* **1996**, *100*, 7617–7622.
(30) Conboy, J. C.; Messmer, M. C.; Richmond, G. L. *Langmuir* **1998**, *14*, 6722–6727.
(31) Calvez, E. L.; Blaudez, D.; Buffeteau, T.; Desbat, B. *Langmuir* **2001**, *17*, 670–674.
(32) Kanicky, J. R.; Shah, D. O. *Langmuir* **2003**, *19*, 2034–2038.
(33) Mukerjee, P., Mysels, K. J., Eds. *Critical Micelle Concentrations of Aqueous Surfactant Systems*; U.S. Dept. of Commerce: National Bureau of Standards: Washington, DC, 1971.
(34) Rosen, M. J. *Surfactants and Interfacial Phenomena*, 3rd ed.; Wiley: New York, 2004.
(35) Colthrup, N. B.; Daly, L. H.; Wiberley, S. E. *Introduction to Infrared and Raman Spectroscopy*; Academic Press: New York, 1964.
(36) Bain, C. D.; Davies, P. B.; Ong, T. H.; Ward, R. N. *Langmuir* **1991**, *7*, 1563–1566.
(37) Hore, D. K.; Walker, D. S.; Mackinnon, L.; Richmond, G. L. *J. Phys. Chem. C* **2007**, *111*, 8832–8842.
(38) Hore, D. K.; Walker, D. S.; Richmond, G. L. *J. Am. Chem. Soc.* **2008**, *130*, 1800–1801.
(39) Peterson, P. B.; Saykally, R. J. *J. Phys. Chem. B* **2005**, *109*, 7976–7980.
(40) Buch, V.; Milet, A.; Vacha, R.; Jungwirth, P.; Devlin, J. P. *Proc. Natl. Acad. Sci.* **2007**, *104*, 7342–7347.
(41) Baldelli, S.; Schnitzer, C.; Shultz, M. J. *J. Chem. Phys.* **1998**, *108*, 9817–9820.
(42) Hopkins, A. J.; Mcfearin, C. L.; Richmond, G. L. *J. Phys. Chem. C* DOI: 10.1021/jp202254u.
(43) Gragson, D. E.; Richmond, G. L. *J. Phys. Chem. B* **1998**, *102*, 569–576.
(44) Scatena, L. F.; Richmond, G. L. *J. Phys. Chem. B* **2004**, *108*, 12518–12528.
(45) Umemura, J.; Cameron, D. G.; Mantsch, H. H. *J. Phys. Chem.* **1980**, *84*, 2272–2277.
(46) Gericke, A.; Huhnerfuss, H. *Thin Solid Films* **1994**, *74*, 245.
(47) Gericke, A.; Mendelsohn, R. *Langmuir* **1996**, *12*, 758–762.
(48) Tikhonov, A. M.; Schlossman, M. L. *J. Phys. Chem. B* **2003**, *107*, 3344–3347.
(49) Tikhonov, A. M.; Pingali, S. V.; Schlossman, M. L. *J. Chem. Phys.* **2004**, *120*, 11822–11838.